Holographic Phase Retrieval of RF-EMFs for Human Exposure Assessment using Fine 3D Electric Field Measurements in a Real Environment from a Beamforming 28 GHz Antenna

Robin Wydaeghe, Olivier Caytan, Sergei Shikhantsov, Emmeric Tanghe,
Günter Vermeeren, Hendrik Rogier, Sam Lemey, Piet Demeester, Wout Joseph

Department of Information Technology, Ghent University/IMEC,
WAVES & IDLab, Ghent, Belgium. Corresponding author: Robin.Wydaeghe@UGent.be.

***Abstract*—With the increasing frequencies for 5G and 6G technology, accurate assessment of Radio-Frequency Electromagnetic Fields (RF-EMFs) on humans is crucial for compliance with safety guidelines. Matching measurement results with simulations is challenging due to the loss of phase information and the need for high-fidelity digital twins of complex environments. In this paper, we propose a novel holographic phase retrieval method based on fundamental electromagnetics, utilizing the Gerchberg–Saxton algorithm, to reconstruct the full electric and magnetic vector fields in real environments from phaseless measurements. The exposure can be computed using a Huygens' box method. We conducted fine-grained 3D electric field measurements using a calibrated probe in a real environment illuminated by a beamforming 28 GHz antenna. Although the algorithm did not converge in the complex real-world environment, we validated the feasibility of our method with a proof-of-concept at 3.5 GHz. The results demonstrate interference patterns and suggest that, with further refinement, the proposed approach can be effective for human exposure assessment in realistic scenarios.**

***Index Terms*—EMF exposure, holographic phase retrieval, RF-EMF measurements, exposure assessment, beamforming, Gerchberg–Saxton algorithm, 5G mmWave, digital twin, 3D field measurements, phase reconstruction**

I. Introduction

With the advent of 5G and 6G, both measurements and simulations are performed to assess the exposure of Radio-Frequency Electromagnetic Fields (RF-EMFs) on humans at increasingly higher frequencies, such as 5G's FR2 band around 28 GHz. Measurements commonly constitute field campaigns with a free-space calibrated electric field probe and spectrum analyzer. By performing measurements with this probe in real environments, researchers can determine if the electric fields are within the ICNIRP guidelines [1]. This data is *expensive* as it requires manual labor. It can be characterized as high accuracy but with low precision. On the other hand, simulations can model realistic Electromagnetic Fields (EMFs) with advanced propagation models such as (differentiable) ray tracing [2]. These can be interfaced with exposure assessment techniques [3] for the determination of absorption quantities, an advantage measurements do not possess. This data is *low-cost* as large quantities can be obtained. It can be characterized as low accuracy but high precision. Matching the results from a measurement perfectly with those from a simulation has never been achieved in real environments at the mmWaves and sub-THz frequencies envisioned for 5G and 6G due to difficulties on both sides of the comparison.

On the measurement side, determining the phase of an electromagnetic wave requires complex synchronization with the transmitter. Also, the positioning of the equipment must be accurate by no more than a couple of millimeters. The environment must also be completely static during the measurement.

On the simulation side, a digital twin is required with features accurately modeled within a couple of millimeters. The underlying propagation model should incur as few assumptions as possible and must be correctly parameterized. For example, ray-tracing simulations use estimates for a material's electric parameters and its diffusivity response. In [4], this is "learned" using a differentiable ray-tracer, but large errors remain. Finally, a perfect model for the transmitting and receiving antenna is also needed to obtain the exact same results with measurements.

We achieved a good match in an anechoic room scenario at 28 GHz [5]. In this paper, we measure electric field values in a real environment (a stairwell) with a fine-grained sweep of a 3D domain using a positioning robot. This is performed with a recently released calibrated electric field probe and spectrum analyzer from Narda for 5G's FR2. To the best of the authors' knowledge, this represents a novel contribution in the field of RF-EMFs measurements. We propose here a new method that reconstructs the electric field based solely on phaseless and incomplete measurement data. This electric field can then be computed in the whole 3D domain, for each vector component, with accurate phase information. The method is derived based on fundamental electromagnetics introducing only a far-field condition as assumption. The key phase retrieval algorithm

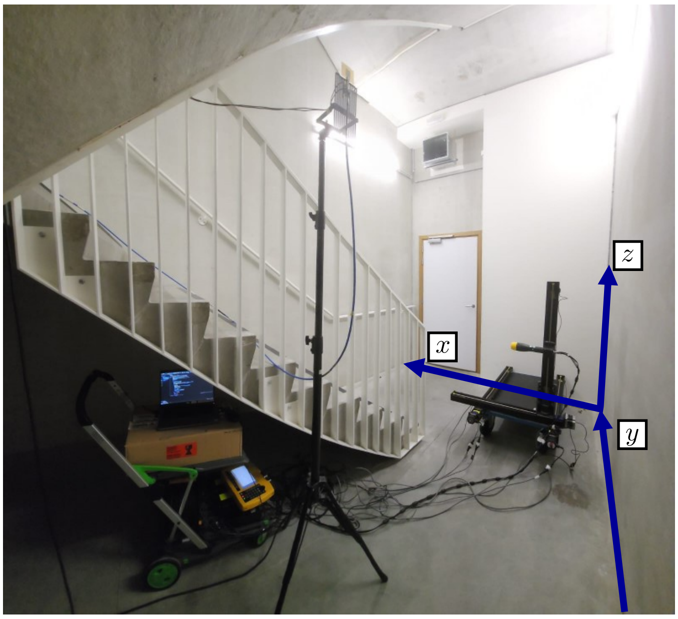

Fig. 1: Wide-angle photograph of the measurement setup. The robot (right) holds the Narda probe (yellow) and moves along the three cartesian directions: x towards the door, y normal to the right wall and z normal to the floor. The antenna (top, center) faces the right wall and radiates toward the setup at an angle.

finds its basis in holographic theory with an application of the Gerchberg–Saxton algorithm [6].

II. Methods

A. Measurement setup

The measurement setup is shown in Fig. 1. The environment is a rectangular room with smooth concrete walls, a door, and a U-shaped stairwell. The measurement takes place to the left of the door, below the second staircase. The y-axis is parallel to the door, pointing from the wall to the staircase. The z-axis points up from the floor and the x-axis is normal to the door, pointing out of the room.

An antenna is mounted on a pole, radiating at 28 GHz at a height of 1.68 m tilting downward with an angle of 11.5°. The antenna, as detailed in [7], consists of 4 antenna elements and a passive Butler Matrix. Here, the first three ports are terminated and the fourth is fed a sinusoidal signal, such that a directed beam is cast toward the measurement setup at an angle of -14° [8].

The measurement is performed similarly as in [5] and first introduced in [9]. A calibrated uniaxial EMF probe measures the magnitude of the longitudinal electric field component. We use the Narda 5G FR2 probe with a bandwidth 26.5 GHz to 29.5 GHz connected to the Narda SRM-3006 [10], which in turn is connected to a computer. The probe is mounted on a 3D positioning robot, consisting of 3 Velmex slides in orthogonal directions. The actuators move with sub-mm precision. The robot and the probe are positioned and mounted to align at 90° angles with the walls of the room. The longitudinal probe direction is therefore aligned with the y-axis.

The SRM-3006 and 3D positioning robot are operated synchronously by a laptop. The SRM-3006, laptop, and all other equipment are placed below the first staircase to minimize the error with the digital twin. The robot traces out a snake-like path covering a 3D domain, while the probe measures continually. The time series of measured field values is mapped to points along the traced path. This approach increases the efficiency substantially compared to [5] and changes the bottleneck of the measurement's duration to the speed of the actuators instead of the probe measurements. Moreover, the resolution is continuous (only limited by the measurement time-interval) along one axis of the snake-like path but discrete along the other two, further referred to as the *discrete-axis resolution*. The 3D domain have a size of 85 cm × 40 cm × 70 cm. For a discrete-axis resolution of $\lambda/4$, it takes 31 hours to measure the 5 slices at $x = 0\,\text{cm}$, $x = 40\,\text{cm}$, $y = 0\,\text{cm}$, $y = 20\,\text{cm}$ and $y = 40\,\text{cm}$.

A digital twin of the environment was carefully constructed. The architectural model of the building was provided to us in Revit and converted to OpenUSD. We verified that the architectural model's distances conformed to the distance measurements in the room. The position of the antenna, the robot, and the probe was measured and located in the digital twin.

B. Holographic Phase Retrieval method

To compute the theoretical exposure on a human of the antenna, the EMFs $\mathbf{e}(\mathbf{r})$ and $\mathbf{h}(\mathbf{r})$ need to be known in the full 3D domain. However, the measurement only provides $|e_y(\mathbf{r})|$ on certain slices of the 3D domain. We propose an algorithm that reconstructs the full EMFs which match the measured $|e_y(\mathbf{r})|$.

According to the Huygens-Fresnel principle, every wave-front is the sum of a number of spherical wavelets emanating from points in the environment. From Maxwell's equations, the electric field can be expressed as [11]

$$\mathbf{e}(\mathbf{r}) = -j\omega\mu_0 \int_S \overline{\overline{\mathbf{G}}}(\mathbf{r},\mathbf{r}') \cdot \mathbf{j}(\mathbf{r}')\,\mathrm{d}\mathbf{r}' \,, \tag{1}$$

where $\mathbf{j}$ is the current density on the physical features of the environment S. Green's tensor $\overline{\overline{\mathbf{G}}}$ is explicitly given by

$$\overline{\overline{\mathbf{G}}}(\mathbf{r},\mathbf{r}') = \left(\mathbf{I} + \frac{1}{k^2}\boldsymbol{\nabla}\boldsymbol{\nabla}\right) G(R) \,,$$

where $R = \|\mathbf{R}\| = |\mathbf{r}-\mathbf{r}'|$ and $G(R) = -\exp(jkR)/R$. One can prove in the far-field limit that all non-radiative components become negligible and

$$\lim_{kR\to\infty} \overline{\overline{\mathbf{G}}}(\mathbf{r},\mathbf{r}') = \frac{\exp(-jk\,|\mathbf{r}-\mathbf{r}'|)}{4\pi\,|\mathbf{r}-\mathbf{r}'|}\left(\mathbf{I} - \hat{\mathbf{R}}\hat{\mathbf{R}}\right) \,, \tag{2}$$

where $\hat{\mathbf{R}} = \mathbf{R}/|\mathbf{R}|$. The term $\mathbf{I} - \hat{\mathbf{R}}\hat{\mathbf{R}}$ projects the current density onto the plane perpendicular to $\hat{\mathbf{R}}$. Equation (2) locally behaves as a plane wave. The integral in equation (1) can be approximated by a sum over a large number of *scattering clusters* C, assuming $\mathbf{r}$ is in the far-field of each cluster, as:

$$\mathbf{e}(\mathbf{r}) \approx \sum_{c=0}^{C} \left(a_c^\theta \hat{\mathbf{u}}_c^\theta(\mathbf{r}) + a_c^\phi \hat{\mathbf{u}}_c^\phi(\mathbf{r}) \right) \frac{\exp(-jk\,|\mathbf{r}-\mathbf{r}_c|)}{|\mathbf{r}-\mathbf{r}_c|}\,, \quad (3)$$

where θ and ϕ denote the polarizations along the spherical unit vectors, $a_c^{\theta/\phi}$ represents the θ and ϕ *coefficients* of cluster c, $\hat{\mathbf{u}}_c(\mathbf{r})$ is the polarization unit vector of the vector connecting the cluster at $\mathbf{r}_c$ with $\mathbf{r}$. For an infinite amount of clusters padding the surface S completely, the coefficients of a specific cluster c represent the amplitude and phase of the current density $-j\omega\mu_0\mathbf{j}(\mathbf{r}')$, projected onto the polarization axes $\hat{\mathbf{u}}_c^{\theta/\phi}$ of c.

Finding the EMFs entails finding the coefficients of all the clusters $a_c^{\theta/\phi}$. The vectors $\mathbf{a}^\theta$ and $\mathbf{a}^\phi$ collect all these coefficients for the θ and ϕ polarizations, respectively. We consider K points $\mathbf{r}_i$ where measurements of the electric field are known. As only the y-component is measured, we premultiply (3) by $\hat{\mathbf{u}}_y$ and write this in matrix notation

$$\underbrace{\hat{\mathbf{u}}_y \cdot \begin{bmatrix} \mathbf{e}(\mathbf{r}_1) \\ \vdots \\ \mathbf{e}(\mathbf{r}_K) \end{bmatrix}}_{\mathbf{y}} = \underbrace{\hat{\mathbf{u}}_y \cdot \begin{bmatrix} \overline{\overline{\mathbf{H}}}^\theta & \\ & \overline{\overline{\mathbf{H}}}^\phi \end{bmatrix}}_{\mathbf{H}} \underbrace{\begin{bmatrix} \mathbf{a}^\theta \\ \mathbf{a}^\phi \end{bmatrix}}_{\mathbf{x}}, \quad (4)$$

where the elements of the $\overline{\overline{\mathbf{H}}}^{\theta/\phi}$ tensors are

$$\mathbf{h}_{ic}^{\theta/\phi} = \frac{\exp(-jk\,|\mathbf{r}_i-\mathbf{r}_c|)}{|\mathbf{r}_i-\mathbf{r}_c|} \mathbf{e}_c^{\theta/\phi}(\mathbf{r}_i)\,. \quad (5)$$

Equation (4) can be solved for the cluster coefficients in a least-squares sense with the Moore-Penrose pseudoinverse [12], [13]:

$$\begin{aligned} \mathbf{x} &= \mathbf{H}^+\mathbf{y} \\ &= \begin{bmatrix} \mathbf{V}_\theta \mathbf{\Sigma}_\theta{}^+ \mathbf{U}_\theta^H & \\ & \mathbf{V}_\phi \mathbf{\Sigma}_\phi{}^+ \mathbf{U}_\phi^H \end{bmatrix} \mathbf{y}\,, \end{aligned} \quad (6)$$

where the singular value decomposition of the channel matrix $\mathbf{H}^{\theta/\phi} \in \mathbb{C}^{K\times C}$ is used.

Moreover, only the magnitudes $\mathbf{y}^{\text{meas}} = |\mathbf{y}|$ of the y-components are known. Equations (3) and (6) are the spatial forward and inverse Fourier transforms between representations in the *cluster domain* and *field domain*. We propose a holographic phase retrieval method that computes an electromagnetically consistent set of field values whose amplitudes converge to the measured values. This is based on the Gerchberg–Saxton algorithm [6] and is described in Algorithm 1. The resulting cluster coefficients are used in (3) to compute $\mathbf{e}(\mathbf{r})$ (and trivially $\mathbf{h}(\mathbf{r})$) everywhere in the 3D domain.

C. Exposure assessment

To assess the exposure on humans, the same approach as in [3] is used. The head of the MIDA anatomical phantom [14] is used to evaluate the exposure at 28 GHz. On the bounding box of this head, the EMFs are evaluated. This forms the input of a Huygens' box in a Total-Field/Scattered-Field formulation. Using Sim4Life V8.0, a harmonic FDTD simulation at 28 GHz yields the absorption of the EMFs inside the phantom. In a post-processing step, the basic quantity S_{ab} is computed according to the IEEE/IEC 63195-2-2022 standard.

Algorithm 1 Holographic Phase Retrieval with the Gerchberg–Saxton Algorithm

Input: Channel matrix $\mathbf{H}$, measured fields $\mathbf{y}_{\text{meas}}$, convergence threshold $\varepsilon_{\text{conv}}$
Initialize: $n \leftarrow 0$, $\mathbf{x}^{(1)} \leftarrow \mathbf{H}^+\mathbf{y}_{\text{meas}}$ ▷ Measured values have no phase
while $\varepsilon^{(n)} \geq \varepsilon_{\text{conv}}$ **do**
  $\mathbf{y}_{\text{sim}}^{(n)} \leftarrow \mathbf{H}\mathbf{x}^{(n)}$ ▷ Forward Fourier Transform
  for $i = 1, \ldots, K$ **do**
    $y_i^{(n)} \leftarrow |y_{\text{meas}}|\, y_{i,\text{sim}}^{(n)} / \left| y_{i,\text{sim}}^{(n)} \right|$
  end for
  $\mathbf{x}^{(n+1)} \leftarrow \mathbf{H}^+\mathbf{y}^{(n)}$ ▷ Inverse Fourier Transform
  $\varepsilon^{(n)} \leftarrow \left\| \mathbf{y}^{(n)} - \mathbf{y}_{\text{meas}} \right\| / \left\| \mathbf{y}_{\text{meas}} \right\|$
  $n \leftarrow n + 1$
end while
Output: $\mathbf{x}^{(n)}$

III. Results

A. Measurement results

The measured electric field for the slice in the xz-plane at $y = 40\,\text{cm}$ is shown in Fig. 2. A complex interference pattern can be seen. Sets of repeating fringes are seen with varying directions and spatial wavelengths. Some fringes have a nearly straight curvature, in particular for the upper-right corner. This points to plane waves arising from a set of scattering clusters aligned on a plane such as the walls, floor, or ceiling. Strong incident rays reflect off these surfaces, therefore the coefficients of the scattering clusters on these planes have high amplitudes. Some of the interference fringes have spherical wavefronts or more complex patterns. Large-scale variations in field strength are the influence of the antenna lobes at the transmitter. When examining the fields in a small area indicated by a dashed square, we observe the high resolution along the x-axis and lower resolution along the discrete z-axis, caused by the snake-like path of the robot.

B. Holographic phase retrieval result

The MIMO channel matrix $\mathbf{H}$ is computed efficiently using a GPU-accelerated software package developed in-house. For this, the locations of 1000 receivers $\mathbf{r}_i$ are randomly chosen within the measured slices. The locations of the transmitters $\mathbf{r}_c$ are extracted from the digital twin. Using Blender, all surfaces in Line-of-Sight are determined with the evaluation point in the 3D domain. Poisson disk sampling with Bridson's algorithm [15] is used to select clusters spaced at least 5 cm apart.

1) Proof-of-concept scenario: We propose a proof of concept that validates our method at 28 GHz. A cubic 3D domain of $1\,\text{m}^3$ centered on the origin is considered with a slice through $z = 0\,\text{m}$. 1000 evaluation points (receivers) are placed randomly in this domain. 10 clusters (transmitters)

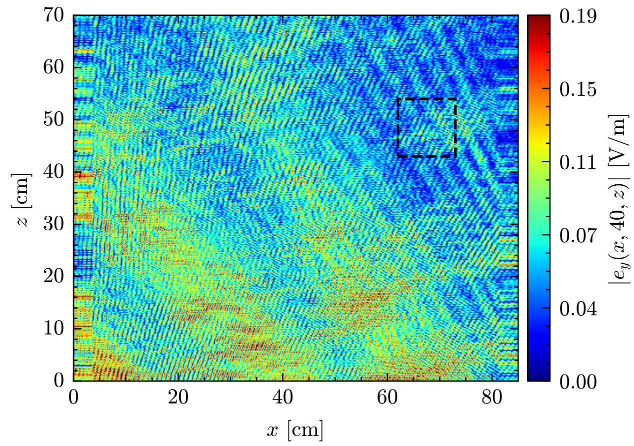

(a) The measured fields in the full slice. A dashed square indicates the area shown in (b).

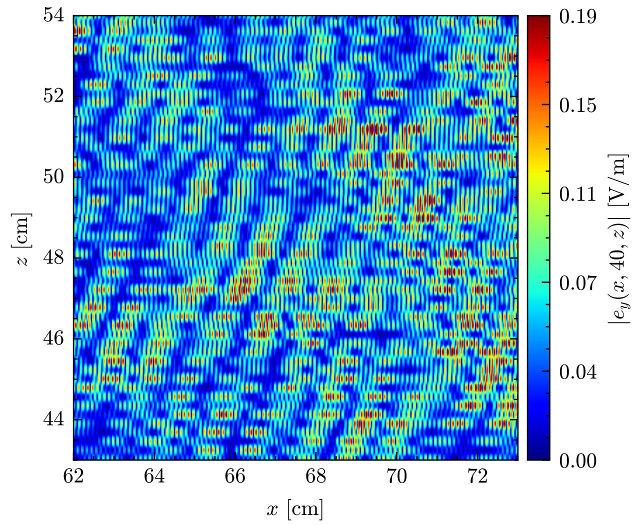

(b) The measured fields in the dashed square shown in (a).

Fig. 2: Measured field values in one of the slices. A calibrated electric-field probe measures the magnitude of the electric field in its longitudinal component (the y-axis) in a slice at $y = 40\,\mathrm{cm}$ at 28 GHz. To improve the visual dynamic range, the maximum shown field value is the 95$^{\mathrm{th}}$-percentile of the actual field value.

are randomly placed at a distance of 1 m from the domain's center. A reference scenario is computed and $\mathbf{H}$ and $\mathbf{H}^{+}$ are determined. Then, a *scrambled scenario* is considered, where the distance of the clusters is randomly extended from the center of the domain by [0, 1) cm. Moreover, the elements of $\mathbf{A}$ are scrambled with random numbers on the unit disk. We take the magnitude of the y-component of the resulting measured electric as the only known quantity and retrieve the original fields and cluster coefficient using our method. In Figure 3, the error $\varepsilon^{(n)}$ is plotted until a convergence of 1% is reached. The field patterns between the scrambled and reconstructed scenarios are visually identical.

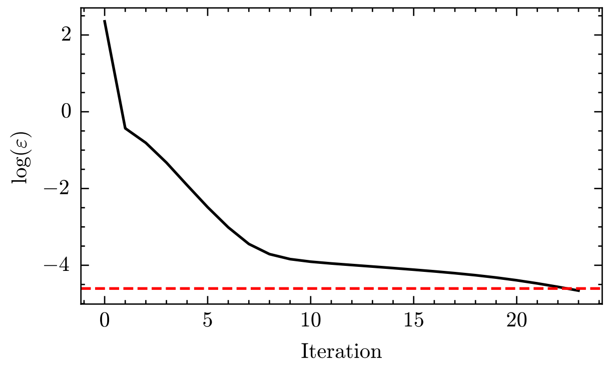

Fig. 3: Error convergence of the proof-of-concept scenario. The red dashed line represents the minimal convergence error (1%).

2) Real environment: The algorithm did not converge to a solution for the realistic case. The mean amplitudes over the whole slices between measured and simulated fields have a deviation of 28%. The phase does not match and therefore also the interference fringes. There are many reasons that could explain this deviation. First, the evaluation points are not in the far-field of scatterers in the room. Most prominently, the robot consists of reflective metallic objects within several centimeters distance from some evaluation points. The Fraunhofer distance $2D^2/\lambda$ with $D = 4.5\,\mathrm{cm}$, a characteristic length of the slides, is 37.8 cm. Second, the digital twin is not accurate enough. The millimeter level of precision required by the small wavelengths of FR2 makes it difficult to align the real with the simulated 3D model. While we expect our algorithm to allow many solutions (because the least-squares problem is underdetermined with $K \ll C$), large differences may still make convergence impossible. Finally, the Narda probe is calibrated in free space and not in this realistic environment. The proximity of metal near the probe could alter its accuracy.

IV. Conclusion

In this study, we presented fine-grained 3D electric field measurements at 28 GHz in a real-world environment, using a calibrated electric field probe mounted on a 3D positioning robot. Over a period of 31 hours, we measured five slices of a 3D domain sized $85\,\mathrm{cm} \times 40\,\mathrm{cm} \times 70\,\mathrm{cm}$, capturing detailed interference patterns that provide valuable insights into the behavior of RF-EMFs at mmWave frequencies. These raw measured fields represent a novel contribution to the field of RF-EMF exposure assessment, particularly at the high frequencies associated with 5G technologies.

We also proposed a holographic phase retrieval method based on the Gerchberg–Saxton algorithm to reconstruct the full electric and magnetic fields from phaseless measurements. While the algorithm did not converge under the complex conditions of the real environment—possibly due to factors such as near-field effects and limitations in the digital twin's accuracy—a proof of concept at 3.5 GHz demonstrated the feasibility of the approach. The error convergence in the proof-of-concept scenario reached the minimal threshold of 1% within 23 iterations, validating the method's potential.

Our findings present an important step toward reconstructing electromagnetic fields in realistic scenarios. The extensive measurement data collected at 28 GHz can serve as a valuable resource for further research. Future work will focus on refining the phase retrieval method, with the goal of matching the simulation with measurements and ultimately assessing the human exposure assessments in complex environments at mmWave frequencies.

V. Acknowledgements

This work was supported by the ERC through *ATTO: A New Concept for Ultrahigh Capacity Wireless Networks* under Grant 695495 and Methusalem through *SHAPE: Next Generation Wireless Networks*. The authors thank EVR architects for providing the 3D model of the building where the measurement took place.

References

[1] ICNIRP, "Guidelines for limiting exposure to electromagnetic fields (100 kHz to 300 GHz)," Health Phys., vol. 118, no. 5, pp. 483-524, Mar. 2020, doi: 10.1097/HP.0000000000001210.

[2] J. Hoydis *et al.*, "Sionna RT: Differentiable Ray Tracing for Radio Propagation Modeling", arXiv preprint arXiv:2303.11103v2, 2023.

[3] R. Wydaeghe *et al.*, "Hybrid Ray-Tracing-QuaDRiGa/FDTD for Realistic mmWave Exposure Assessment with Cell-Free MaMIMO in 3D Outdoor Environments," unpublished.

[4] J. Hoydis *et al.*, "Learning Radio Environments by Differentiable Ray Tracing", arXiv preprint arXiv:2311.18558v1, 2023.

[5] R. Wydaeghe *et al.*, "New Hybrid Ray-Tracing/FDTD for EMF Exposure in 6G Networks using Semantically Classified Google Earth Photogrammetry with Measurement Validation," in Proc. European Conf. Antennas Propag. (EuCAP), Glasgow, Scotland, Mar. 2024.

[6] R. W. Gerchberg and W. O. Saxton, "A practical algorithm for the determination of the phase from image and diffraction plane pictures," Optik, vol. 35, pp. 237–246, 1972.

[7] I. L. de Paula, "Cost-Effective High-Performance Air-Filled SIW Antenna Array for the Global 5G 26 GHz and 28 GHz Bands," IEEE Antennas Wirel. Propag. Lett., vol. 20, no. 2, pp. 194-198, Dec. 2020.

[8] L. Van Messem, "A 4 × 4 Millimeterwave-Frequency Butler Matrix in Grounded Co-Planar Waveguide Technology for Compact Integration With 5G Antenna Arrays," IEEE Trans. Microw. Theory Tech., vol. 71, no. 1, pp. 122-134, Jun. 2022.

[9] S. S. Shikhantsov *et al.*, "Calibrated measurements of the EMF enhancement in the downlink of a 6G distributed antenna array testbed," presented at the URSI General Assembly and Scientific Symposium, Sapporo, Japan, Aug. 2023.

[10] Narda Safety Test Solutions, "Measurement of 5G NR FR2 Electromagnetic Fields," Pfullingen, Germany, Rep. NSTS 0922-E0377B.

[11] J. D. Jackson, "Classical Electrodynamics," 3rd ed., New York, NY, USA: Wiley, 1999.

[12] R. Penrose, "A Generalized Inverse for Matrices," *Proc. Cambridge Philos. Soc.*, vol. 51, no. 3, pp. 406–413, 1955.

[13] G. H. Golub and C. F. Van Loan, *Matrix Computations*, 4th ed. Baltimore, MD, USA: Johns Hopkins Univ. Press, 2013.

[14] M. I. Iacono et al., "MIDA: A Multimodal Imaging-Based Detailed Anatomical Model of the Human Head and Neck," Public Library of Science, vol. 10, no. 4, pp. 1-35, 2015, 10.1371/journal.pone.0124126.

[15] R. Bridson, "Fast Poisson disk sampling in arbitrary dimensions," *ACM SIGGRAPH 2007 Sketches*, San Diego, California, USA, 2007, pp. 22–es. doi: 10.1145/1278780.1278807.